COMSOL CONFERENCE 2024 FLORENCE

Top-Blown Rotary Converter Preheating and Charge Heating with an Oxy-Fuel Burner

Sergey Semenov[1], Patrick Namy[1], Aditya Kale[2], Sello Tsebe[2]
1. SIMTEC, Grenoble, France.
2. MINTEK, Randburg, South Africa.

Abstract
Present work is done in the framework of the SisAl Pilot EU project, which aims at optimising the silicon production in Europe by recycling materials and using a carbon-emission friendly technology. The silicon production experiments are conducted on laboratory and pilot scales in different types of furnaces, including top-blown rotary converters (TBRC) used as chemical reactors for molten slag-metal mixtures. Besides experimental work, the process optimisation also relies on the numerical modelling. In this work COMSOL Multiphysics® is used for the numerical testing of a new thermal design of TBRC by simulating its preheating and charge heating in it due to an external heat source provided by an oxy-fuel burner. The risk of slag solidification in TBRC during aluminothermic reduction of silica was assessed. The following COMSOL® modules are employed: Heat Transfer in Solids and Fluids with phase change, Surface-to-Surface Radiation, and Turbulent Flow k-ω model to simulate the slag and metal flow. A bidirectional coupling of all the modules is present due to multiple interdependencies via material properties. The model predicts that, with 600 kW of the useful burner power, the empty TBRC can be preheated up to 1650°C in less than 30 min. Thanks to the model, the optimum burner power for maintaining the TBRC charge in a liquid state is determined. The influence of TBRC inclination angle as well as of its rotation frequency is studied numerically. The presented modelling approach for testing new TBRC designs can be applied to other similar thermal problems.

Keywords: Top-Blown Rotary Converter, Furnace Preheating, Charge Heating.

1. Introduction
This work is done in the framework of the SisAl Pilot EU project, which is focussed on demonstrating the possibility of metallurgical grade silicon production at pilot scale based on aluminothermic reduction of silica. In comparison with the traditional carbothermic reduction of silica, the advantage of the proposed technology is in its low CO2 emission. As part of the project, the numerical modelling support of experimental works is stipulated. One of the efforts is focussed on developing a numerical model of a top-blown rotary converter (TBRC) heated by an oxy-fuel burner. This metallurgical reactor for the aluminothermic reduction of silica is proposed by MINTEK as an alternative to an electric furnace in order to mitigate the risks associated with the interruption of the electrical power supply due to load shedding in South Africa. Molten slag (50wt%CaO-50wt%SiO_2) and aluminium are planned to be prepared in separate furnaces outside of TBRC and then to be poured into TBRC for the aluminothermic reduction to take place. The objective of the present modelling work is to test the thermal performance of TBRC during the preheating and the aluminothermic reduction stages. The risk of slag solidification in TBRC during aluminothermic reduction stage needs to be assessed. The optimum burner power for maintaining the TBRC charge in a liquid state is to be determined. The influence of TBRC inclination angle as well as of its rotation frequency should be also studied numerically. In sections 2 and 3, model geometry and numerical methods are described. Sections 4 and 5 present governing equation and material properties. In section 6, numerical results are presented and discussed. Section 7 concludes the work.

2. Problem geometry
The geometry and dimensions of the top-blown rotary converter (TBRC) are based on technical drawings provided by MINTEK. The corresponding numerically modelled axisymmetric geometry of TBRC and materials are shown in Figure 1. The steel shell is not modelled because its geometry is not known prior to the furnace construction, as well as because its contribution to the wall's thermal resistance is insignificant due to high thermal conductivity of steel and due to relatively small shell thickness. The heights H_s and H_m of respectively slag and metal layers inside of TBRC are modelled based on the materials' initial volumes $V_{0,s}$ and $V_{0,m}$ and on the geometry of TBRC's internal cavity that depends on the spatial orientation of TBRC. Two TBRC orientations are numerically modelled in this work: vertical orientation, see Figure 2 (a), and

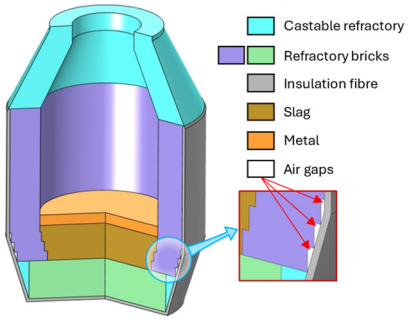

Figure 1. Modelled axisymmetric geometry of TBRC.

hypothetical horizontal orientation, see Figure 2 (b). The initial volumes $V_{0,s}$ and $V_{0,m}$ of correspondingly slag and metal are computed from their given initial masses $m_{0,s} = 500$ kg and $m_{0,m} = 150$ kg and their initial densities $\rho_{0,s}(T_{0,s}, \mathbf{X}_{0,s})$ and $\rho_{0,m}(T_{0,m}, \mathbf{X}_{0,m})$ that depend on their initial temperatures $T_{0,s}$ and $T_{0,m}$ and initial compositions $\mathbf{X}_{0,s}$ and $\mathbf{X}_{0,m}$.

$$V_{0,k} = m_{0,k}/\rho_{0,k}(T_{0,k}, \mathbf{X}_{0,k}), \qquad k = s, m$$
$$\mathbf{X}_{0,s} = (X_{0,SiO_2}, X_{0,Al_2O_3}, X_{0,CaO})$$
$$\mathbf{X}_{0,m} = (X_{0,Si}, X_{0,Al}, X_{0,Ca})$$

where subscripts s and m stand for slag and metal, $X_{0,i}$ stands for an initial mole fraction of species i.

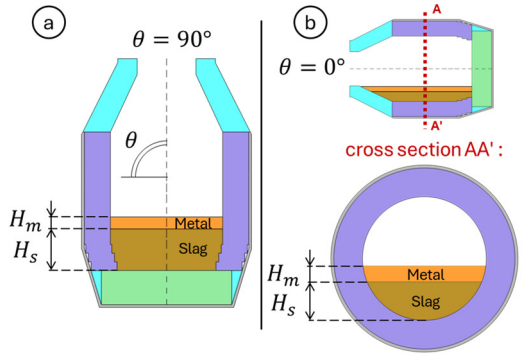

Figure 2. Numerically modelled orientations of TBRC. (a): Vertical orientation. (b): Horizontal orientation.

3. Numerical methods

The problem is solved with the finite element software COMSOL Multiphysics® version 6.1. The modules of Heat Transfer, Turbulent Flow k-ω, and Surface-to-Surface Radiation have been used to set up the model physics. Temperature and velocity fields are spatially discretized with quadratic elements, whereas pressure and surface radiosity are discretized with linear elements. Time integration is performed with the Backward Differentiation Formula (BDF) of order 1 to 2. The computational domain is spatially discretized with a triangular mesh that consists of 27 600 finite elements, see Figure 3, resulting in 220 700 degrees of freedom. The computations are performed on 2 laptops with 8 physical cores Intel processor, 64 GB RAM, and a workstation with 64 physical cores and 1 TB RAM.

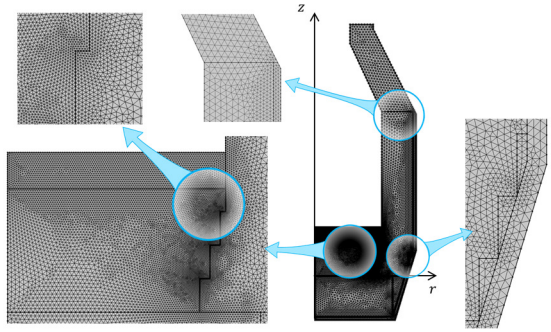

Figure 3. Computational mesh.

4. Governing Equations

The physics of the problem includes heat transfer in solids and fluids with phase change, surface-to-surface radiation, and turbulent k-ω model to simulate slag and metal flow. All transport equations and boundary conditions are similar for both vertical and horizontal orientations of TBRC. Without loss of generality, only the vertical configuration is presented in this section.

4.1. Fluid dynamics in metal phase

Unsteady incompressible RANS equations with k-ω turbulence model are solved in the metal domain:

$$\rho(\partial\mathbf{u}/\partial t + \mathbf{u}\cdot\nabla\mathbf{u}) = \nabla\cdot[-p\mathbf{I} + \mathbf{K}] + \rho\mathbf{g}$$
$$\nabla\cdot\mathbf{u} = 0, \qquad \mathbf{K} = (\mu + \mu_T)(\nabla\mathbf{u} + (\nabla\mathbf{u})^{\mathsf{T}})$$
$$\rho(\partial k/\partial t + \mathbf{u}\cdot\nabla k) = \nabla\cdot[\mu_k\nabla k] + P_k - \beta_0^*\rho\omega k$$
$$\rho\left(\frac{\partial\omega}{\partial t} + \mathbf{u}\cdot\nabla\omega\right) = \nabla\cdot[\mu_\omega\nabla\omega] + \alpha\frac{\omega}{k}P_k - \beta_0\rho\omega^2$$
$$\mu_T = \rho k/\omega, \quad \mu_k = \mu + \mu_T\sigma_k^*, \quad \mu_\omega = \mu + \mu_T\sigma_\omega$$
$$P_k = \mu_T[\nabla\mathbf{u}:(\nabla\mathbf{u} + (\nabla\mathbf{u})^T)], \quad \alpha = 0.52$$
$$\sigma_k^* = 0.5, \quad \sigma_\omega = 0.5, \quad \beta_0 = 0.072, \quad \beta_0^* = 0.09$$

In this model, a turbulent viscosity μ_T is calculated from two additional fields, the turbulent kinetic energy k and the specific rate of dissipation of turbulent kinetic energy ω. The condition of axial symmetry is applied at $r = 0$:

$$u_r = 0, \ \partial\zeta/\partial r = 0, \ \text{where } \zeta = u_r, u_z, p, k, \omega$$

Slip boundary condition on the upper metal surface:

$$\mathbf{u}\cdot\mathbf{n} = 0, \ \mathbf{K_n} - (\mathbf{K_n}\cdot\mathbf{n})\mathbf{n} = 0, \ \mathbf{K_n} = \mathbf{K}\cdot\mathbf{n}$$
$$\nabla k\cdot\mathbf{n} = 0, \ \nabla\omega\cdot\mathbf{n} = 0$$

No-slip condition is imposed on the metal-slag (MS) and the metal-refractory (MR) interfaces. Metal moves tangentially to the interface with the velocity of slag $\mathbf{u}_s$ at the MS interface or with the velocity of rotating refractory $\mathbf{u}_{rot}$ at the MR interface due to TBRC rotation about its axis of symmetry:

$$\mathbf{u}\cdot\mathbf{n} = 0, \ \mathbf{K}\cdot\mathbf{n} = -\rho u^* u_\tau \mathbf{u}_\tau/|\mathbf{u}_\tau|, \ \nabla k\cdot\mathbf{n} = 0$$
$$\omega = (\omega_{visc}^2 + \omega_{log}^2)^{1/2}$$
$$\omega_{visc} = 6\mu/(\rho\beta_0\delta_w^2), \qquad \omega_{log} = u^*/(\kappa_v\delta_w\sqrt{\beta_0^*})$$
$$\mathbf{u}_\tau = \mathbf{u}_{rel} - (\mathbf{u}_{rel}\cdot\mathbf{n})\mathbf{n}, \qquad \mathbf{u}_{rel} = \mathbf{u} - \mathbf{u}_{bnd},$$
$$\mathbf{u}_{bnd} = \begin{cases}\mathbf{u}_s, & \text{at MS interface}\\ \mathbf{u}_{rot}, & \text{at MR interface}\end{cases}$$
$$u_{rot,r} = 0, \ u_{rot,\varphi} = r\omega_{rot}, \ u_{rot,z} = 0$$
$$u^* = \left[u_{\tau,visc}^4 + (u_{log}^*)^4\right]^{\frac{1}{4}}, \ u_\tau = \left[u_{\tau,visc}^4 + u_{\tau,log}^4\right]^{\frac{1}{4}}$$
$$u_{log}^* = \sqrt{\max(0,k)\sqrt{\beta_0^*}}, \ u_{\tau,visc} = \sqrt{\mu|\mathbf{u}_\tau|/(\rho\delta_w)}$$
$$u_{\tau,log} = |\mathbf{u}_\tau|\kappa_v/(\ln[\max(1,\delta_w^+)] + B\kappa_v)$$
$$\delta_w^+ = \rho u^*\delta_w/\mu, \ \kappa_v = 0.41, \ B = 5.2$$

where $\mathbf{n}$ is unit normal vector at the interface, ω_{rot} is the angular velocity of TBRC rotation, and δ_w is the wall lift-off distance that equals half of the size of the near-wall element. Ambient pressure p_{amb} is imposed at the right top corner of the metal domain.

4.2. Fluid dynamics in slag phase

Similar unsteady incompressible RANS equations with k-ω turbulence model are also solved in the slag domain. The only difference is that in the solid or porous phase of slag, the Darcy force $\mathbf{f}_D$ is added:

$$\mathbf{f}_D = -\mu(\mathbf{u} - \mathbf{u}_{rot})/K_{perm}$$

where μ is the intrinsic slag viscosity and K_{perm} is the slag permeability (Kozeny-Carman model):

$$K_{perm} = K_0\, g_l^3/(1 - g_l)^2$$

with $K_0 = 7 \times 10^{-9}\,\mathrm{m}^2$ and g_l being the liquid fraction. Additional source terms related to the Darcy force are also added in the right hand side of turbulence equations [1]: $-2\,\mu k/K_{perm}$ in the k equation and $-2\,\mu\omega/K_{perm}$ in the ω equation. The boundary condition of tangential stress and zero normal velocity is applied at the slag-metal interface:

$$\boldsymbol{\sigma}_{\tau,slag} = \boldsymbol{\sigma}_{\tau,metal},\ \ \boldsymbol{\sigma}_\tau = \boldsymbol{\sigma} - (\boldsymbol{\sigma}\cdot\mathbf{n})\mathbf{n}$$

$\boldsymbol{\sigma} = [-p\mathbf{I} + \mathbf{K}]\cdot\mathbf{n}$ (same $\mathbf{n}$ for both slag and metal)

$$\mathbf{u}\cdot\mathbf{n} = 0,\ \ \nabla k\cdot\mathbf{n} = 0,\ \ \nabla\omega\cdot\mathbf{n} = 0$$

the use of which is justified by the fact that slag comes into motion due to shear stress of the tangential metal flow above it, while the interface displacement in normal direction is neglected. No-slip condition at the slag-refractory interface and the axial symmetry condition at $r = 0$ are imposed with equations similar to those from the previous subsection. Hydrostatic pressure of metal layer is applied at the right top corner of the slag domain.

4.3. Heat transfer with surface-to-surface radiation

The following heat equation is solved in all domains:

$$\rho c_p'(\partial T/\partial t + \mathbf{u}\cdot\nabla T) + \nabla\cdot\mathbf{q} = 0$$

$$\mathbf{q} = -(k + k_T)\nabla T$$

where T is temperature, ρ is density, c_p' is the specific heat capacity at constant pressure modified according to the Apparent Heat Capacity method to account for phase changes, $\mathbf{u}$ is velocity, $\mathbf{q}$ is conductive heat flux, k and k_T are respectively molecular and turbulent thermal conductivity:

$$k_T = c_p\mu_T/\mathrm{Pr}_T$$

where μ_T is the turbulent viscosity, and Pr_T is the turbulent Prandtl number, which is often modelled as a function of the molecular Prandtl number Pr [2]. For simplicity, a constant value of turbulent Prandtl number is adopted in the present numerical study:

$$\mathrm{Pr}_T = 0.85$$

In solid domains, the convective term $(\mathbf{u}\cdot\nabla T)$ and the turbulent conductivity k_T are omitted. In solid phase of the slag layer these terms are suppressed with help of the Darcy force, see subsection 4.2. The condition of axial symmetry at $r = 0$ is:

$$\partial T/\partial r = 0$$

Temperature is continuous on all material interfaces:

$$T_{up} = T_{down}$$

where subscripts up and $down$ denote the upward and downward sides of the interface: up corresponds to the material where unit normal vector $\mathbf{n}$ is pointing to. The condition of heat flux continuity/discontinuity at material interfaces is:

$$\mathbf{q}_{up}\cdot\mathbf{n} - \mathbf{q}_{down}\cdot\mathbf{n} = q$$

where q is the surface density of the interfacial heat source. Boundary heat source provided by an oxy-fuel burner on internal surfaces of TBRC:

$$-\mathbf{q}\cdot\mathbf{n} = q_{burner}$$

where unit normal vector $\mathbf{n}$ at the metal-air or refractory-air interface is pointing into air. Interfacial heat source due to exothermic aluminothermic reaction at the metal-slag interface:

$$-[\mathbf{q}_{slag} - \mathbf{q}_{metal}]\cdot\mathbf{n}_{slag} = q_{reaction}$$

where $\mathbf{n}_{slag}$ is pointing into metal, $q_{reaction}$ is the surface density of reaction power computed from the reaction enthalpy and the reaction time. Heat flux due to external natural convection is applied on external TBRC boundaries:

$$-\mathbf{q}\cdot\mathbf{n} = h(T_{amb} - T)$$

where $\mathbf{n}$ is the outward unit normal vector and h is the heat transfer coefficient, computed according to empirical models of external natural convection. On interfaces and boundaries that participate in the surface-to-surface radiation (all external and internal surfaces of TBRC, as well as interfaces of air gaps), an additional boundary heat source q_r is imposed due to thermal radiation absorption:

$$q_r = \varepsilon(G - \sigma_{SB}T^4)$$

where ε is the hemispherical emissivity of the radiating surface, σ_{SB} is the Stefan-Boltzmann constant, and G is the surface irradiance.

5. Material properties and parameters

5.1. Refractory materials and air

Thermal properties of all refractory materials are provided by MINTEK: VR 90B alumina-silicate is used for the refractory bricks, L-Cast 18 alumina-silicate for the castable refractory, and 1260 ST-RB ceramic fibre blanket for the insulation fibre. The specific heat capacity at constant pressure $c_p(T)$ is approximated based on materials composition:

$$c_p(T) = \textstyle\sum_i \omega_i\, c_{p,i}(T),\ \ i = \mathrm{SiO_2}, \mathrm{Al_2O_3}, \mathrm{etc.}$$

where ω_i is the mass fraction, and $c_{p,i}(T)$ is the specific heat capacity of component i from the NIST database [3]. A constant-value extrapolation of all properties is used for out-of-range temperatures. The air gaps, see Figure 1, are assumed to be filled with air, whose properties are taken from the COMSOL Multiphysics® materials library.

5.2. Slag and metal

In metal phase, initially pure Al becomes an Al-Si-Ca alloy as it reacts with slag. Similarly, initially SiO_2-CaO slag becomes Al_2O_3-SiO_2-CaO slag as it reacts with metal. Thus, slag and metal densities are modelled as functions of temperature T and composition X_i (mole fraction of component i):

$$\rho(T, X_i) = \textstyle\sum_i[X_iM_i]/\left(\sum_i\left[X_iV_{mol,i}(T)\right] + V^{EX}\right)$$

where M_i and $V_{mol,i}$ are respectively the molar mass and the molar volume [4, 5, 6, 7] of component i, V^{EX} is a corrective interaction term [7], $i = \mathrm{Al, Si, Ca}$ for metal and $i = \mathrm{Al_2O_3, SiO_2, CaO}$ for slag. The composition of slag and metal is modelled as function of the relative reaction extent ξ_{rel} that equals 0 at the beginning of the process and 1 at the end of the reaction:

$$X_i = X_{i,init} + \xi_{rel}\left(X_{i,final} - X_{i,init}\right)$$

For simplicity, ξ_{rel} is a linear function of time:

$$\xi_{rel} = t/t_r$$

where t_r is the user defined reaction time. The initial $X_{i,init}$ and final $X_{i,final}$ compositions, as well as the reaction energy, are estimated with help of the software provided by the project partner SINTEF. This artificial-neural-network-based tool [8, 9] is

trained on the FactSage® data for the metal-slag system of interest. Other metal properties, such as thermal and electrical conductivity [4], dynamic viscosity [10], and heat capacity at constant pressure are computed as for pure aluminium. Slag thermal conductivity is assumed to be constant and equal to $1\,\mathrm{W/m/K}$. Slag viscosity is modelled as function of temperature and slag composition according to the mathematical model [9] of Kai Tang from SINTEF. Other slag properties, such as heat capacity, enthalpy and electrical conductivity are computed as functions of temperature and composition according to the Ken Mills model [11].

6. Numerical results and discussion

6.1. TBRC preheating

The unsteady process of empty TBRC preheating with an oxy-fuel burner is numerically modelled. It is found that the surface of refractory bricks (inside of TBRC) can reach the desired temperature of 1650°C in less than 30 minutes when useful burner power equals 600 kW. At the same time, the average bricks temperature stays below 200°C, meaning that refractory volume remains relatively cold with respect to the internal TBRC surface. Further preheating would result in a significant temperature increase: the average temperature of bricks surface reaches 2454°C after 12 hours of preheating. It is found that at steady state (as time goes to infinity) most of the power (81.2%) is lost in form of thermal radiation from the internal surface of TBRC towards ambient environment through the opening at the top of the furnace. Therefore, the use of a furnace lid is recommended to prevent significant heat losses during operations that do not involve charging, tapping or heating with a burner. The TBRC state after 30 minutes of preheating with 600 kW input power, see Figure 4, will serve as initial condition for further computations with a furnace charge.

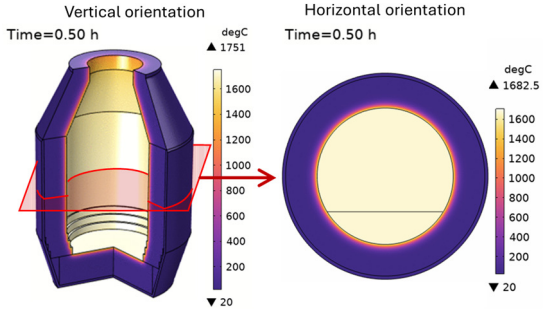

Figure 4. TBRC after 30 min of preheating with 600 kW burner power, initial condition for further computations.

6.2. Influence of TBRC rotation frequency

Let's consider the TBRC charged with only slag that rotates in its horizontal position ($\theta = 0$, see Figure 2). This configuration of the furnace is simulated with a 2D plane model that represents TBRC cross section shown in Figure 2 (b). The initial slag temperature is 1670°C. The initial temperature field in TBRC refractory and air above slag are taken from the earlier solved preheating problem, see Figure 4 (right). The dominant heat transfer mechanism in the air phase is the surface-to-surface radiation. Thus, to simplify the problem, air convection is not solved, only air conduction is considered. The TBRC rotation frequency is initially zero (0 rpm at $t = 0$) and then it smoothly increases up to a given value during first 10 seconds of the simulated process. In the case of full burner power (600 kW) and of the rotation frequency of 5 rpm, the temperature field and slag velocity are shown in Figure 5. The temperature maximum is located on the slag surface exposed to the burner heating, while its minimum is on the external surface of TBRC. The time evolution of slag temperature is shown in Figure 6.

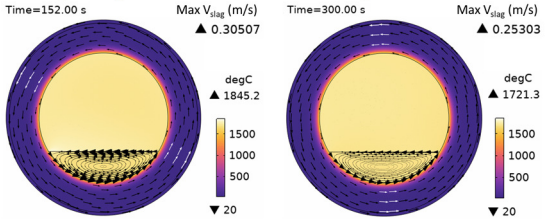

Figure 5. Temperature field and slag velocity at 5 rpm and 600 kW burner power in a horizontal TBRC.

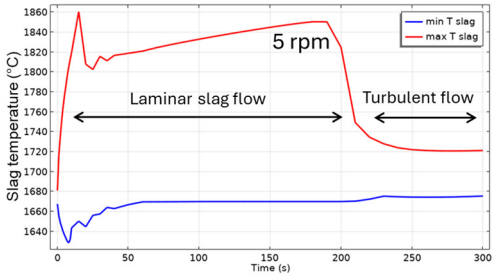

Figure 6. Maximum and minimum slag temperature at 5 rpm and 600 kW burner power in a horizontal TBRC.

For $t < 20$ s, the flow is not yet fully established, resulting in poor stirring. Thus, maximum slag temperature T_{max} quickly rises to 1860°C on its surface heated by the burner, and its minimum temperature T_{min} quickly reduces to 1630°C at the bottom of the slag layer due to heat losses towards ambient environment through the refractory. At $t = 20$ s, when slag flow is fully established, more intensive stirring brings T_{max} down to 1810°C and increases T_{min} up to 1650°C. For $50 < t < 200$ s, T_{max} slowly grows, whereas T_{min} remains almost constant and equal to the initial slag temperature $T_{0,s}$ = 1670°C. This minimum is found in the middle of the flow vortex, where velocity is low, and heat transfer happens primarily by conduction, resulting in slow temperature changes. At 200 seconds there is a qualitative change in the temperature behaviour: the difference between T_{max} and T_{min} suddenly reduces. This is explained by a spontaneous transition to a turbulent flow regime. Indeed, turbulent slag viscosity μ_T is zero for $t < 200$ s and is about 1 Pa·s at $t = 250$ s, whereas intrinsic viscosity μ is 0.117 Pa·s. Turbulence intensifies heat transfer and causes the reduction of temperature difference between T_{max} and T_{min} in the slag layer for $t > 200$ s. When TBRC rotates faster, the

Reynolds number increases, and therefore the spontaneous transition to a turbulent flow regime happens earlier, see 5 to 20 rpm cases in Figure 7.

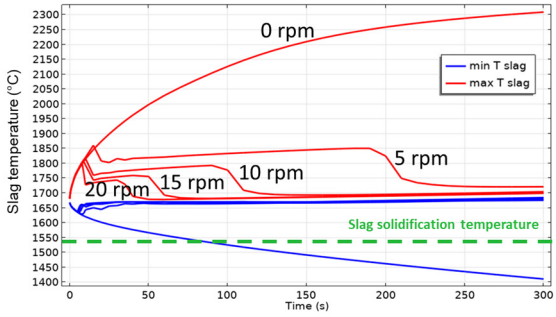

Figure 7. Maximum and minimum slag temperature at different rotation frequencies and 600 kW burner power in a horizontal TBRC.

When TBRC does not rotate, then only natural convection due to buoyancy forces in Earth gravity is present in the slag layer. In this case, slag velocity is much lower as compared to the forced convection case. Thus, poor slag mixing results in a significant temperature difference across the layer (see 0 rpm case in Figure 7) and a slag freezing at the bottom of the pool: see the green dashed line in Figure 7 representing the slag solidification temperature. Let's now consider the influence of rotation frequency in a vertically oriented TBRC ($\theta = 90°$), see Figure 2 (a). Temperature and velocity fields are shown in Figure 8 for 10 rpm rotation frequency at t = 10 and 900 s (note that total simulated duration is 1800 s). Slag velocity in the $r\varphi$ plane reaches 52 cm/s due to furnace rotation, whereas in the rz plane it remains below 0.18 cm/s for $t \geq 900$ s.

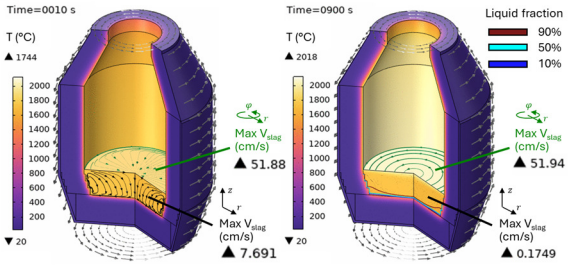

Figure 8. Temperature field and slag velocity at 10 rpm and 600 kW burner power in a vertical TBRC.

This is explained by the fact that in vertical TBRC slag rotates together with TBRC about its axis of symmetry, whereas its vertical position is not perturbed by rotation. In contrast, in the horizontally oriented TBRC, see Figure 5, when furnace rotates, it drags slag up against the gravity force that in turn brings it down to the original level and therefore induces the stirring. Thus, in a vertical TBRC, any rotation frequency is insufficient for the slag stirring and results in a significant temperature difference across the slag layer, see Figure 9. As a result, slag freezing occurs at the bottom of the pool: see the green dashed line in Figure 9 representing the slag solidification temperature and the liquid fraction isolines in Figure 8. Above results show that vertical TBRC orientation is most unfavourable for the slag stirring and leads to its solidification, whereas horizontal TBRC orientation is the most favourable for the stirring and works well as far as furnace rotates, even at 1 rpm.

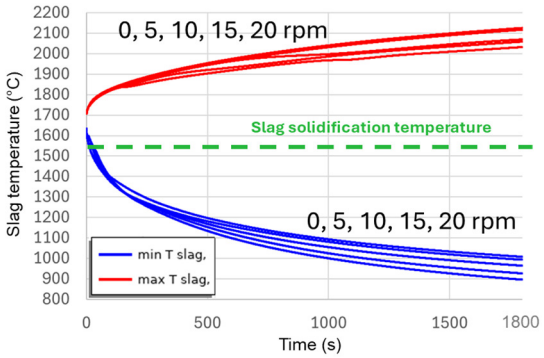

Figure 9. Maximum and minimum slag temperature at different rotation frequencies and 600 kW burner power in a vertical TBRC.

6.3. Influence of the burner power and of TBRC inclination angle

In this subsection, a TBRC charged with slag and metal is numerically modelled, considering an additional heat source at the metal-slag interface due to aluminothermic reduction. First 30 minutes of the process are modelled, keeping in mind that aluminothermic reduction is assumed to last for 20 minutes, followed by 10 minutes of an additional time needed for the TBRC tapping. The objective is to determine the occurrence of slag solidification depending on the burner power and on the TBRC inclination angle. Regarding the last one, vertically oriented TBRC ($\theta = 90°$, see Figure 2) can be modelled with a 2D axisymmetric model, and horizontally oriented one ($\theta = 0°$) with a 2D plane model, whereas any other angle ($0° < \theta < 90°$) requires a full 3D modelling. To be efficient with respect to the computation time, 2D models are prioritized over the 3D ones. Therefore, an interpolation of major quantities of interest between $\theta = 0°$ and 90° is done instead of 3D modelling. Also, only one rotation frequency of 10 rpm, recommended by MINTEK, is modelled here. The temperature and velocity fields in a horizontal TBRC are shown in Figure 10 at 600 kW burner power. The corresponding time evolution of maximum T_{max} and minimum T_{min} slag temperature is shown in Figure 11. At the beginning, T_{min} drops down to 850°C due to direct contact with metal whose initial temperature is 800°C. This causes slag solidification directly under the metal layer, see liquid fraction isolines in Figure 10 at t = 10 s. During next 200 s, due to reaction heat, T_{min} rises back to the initial slag temperature $T_{0,s}$ = 1670°C, see Figure 11. At this point, previously frozen slag is fully remelted without any risk for the furnace operation. Further TBRC heating increases T_{max} at the metal-slag interface up to 2280°C. At the same time, T_{min} in the middle of the bigger laminar convective vortex (see t = 600 s in Figure 10) remains equal to $T_{0,s}$ due to poor mixing. At $t \approx$ 700 s, see Figure 11, a transition

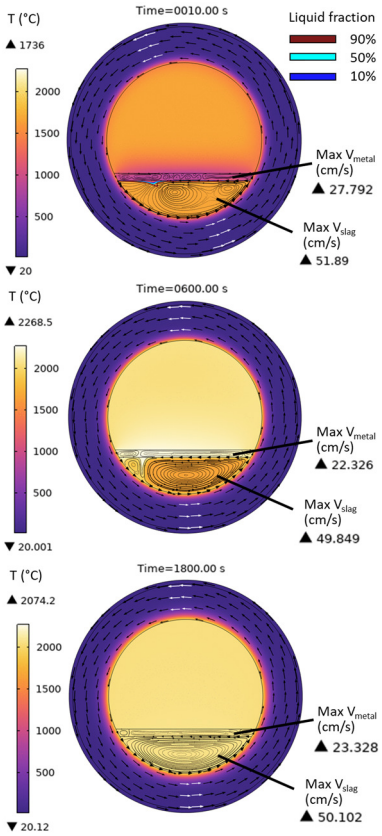

Figure 10. Temperature and velocity fields at 10 rpm and 600 kW burner power in a horizontal TBRC.

to a turbulent flow regime happens in slag, resulting in a significant turbulent thermal conductivity that homogenizes the temperature across the slag layer and brings T_{min} and T_{max} closer together. Further heating increases both T_{min} and T_{max} until the chemical reaction is complete at t = 1200 s. After that, during 1200 s < t < 1800 s, slag temperature is maintained at almost constant value thanks to the operating burner and to the turbulent mixing in the slag layer. Thus, there is no risk of slag solidification if horizontally oriented TBRC operates at 10 rpm and 600 kW burner power. Now let's reduce the burner power. Figure 12 presents T_{min} and T_{max} in a horizontally oriented TBRC at 10 rpm and 164 kW burner power. This is the adjusted burner power that is sufficient to keep slag in a liquid state during first 30 minutes of the process. The transition to a turbulent flow regime does not occur in this case. T_{max} grows up to 2150°C due to reaction heat and then it drops down at 1200 s as reaction stops. T_{min} in the middle of the convective vortex remains equal to $T_{0,s}$ till t = 1700 s, and then it starts to descend due to heat losses but does not reach the solidification temperature T_{sol} = 1540°C during simulated times. So, there is no risk of slag solidification for this furnace configuration. Now, let's remove the burner and see if sole the aluminothermic reduction power is sufficient to keep slag in a liquid state. In this case, the time evolution of slag temperature is shown in Figure 13. As one can see, slag starts to solidify very quickly after the end of reaction, see t = 1500 s in Figure 13. As before, slag temperature in the middle

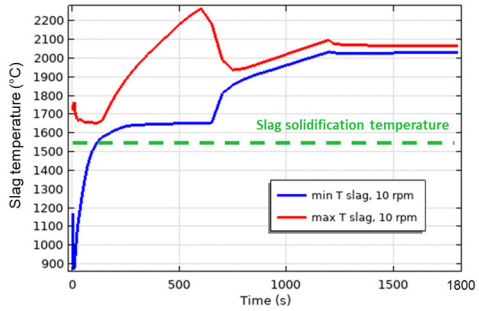

Figure 11. Maximum and minimum slag temperature at 10 rpm and 600 kW burner power in a horizontal TBRC.

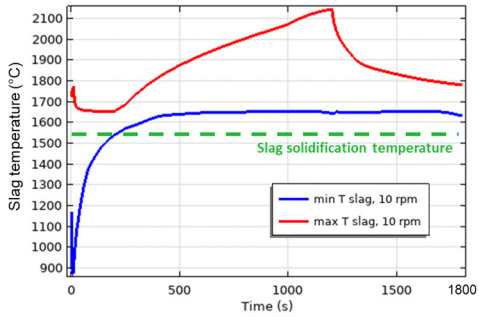

Figure 12. Maximum and minimum slag temperature at 10 rpm and 164 kW burner power in a horizontal TBRC.

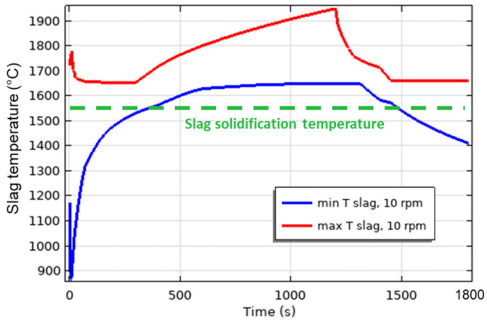

Figure 13. Maximum and minimum slag temperature at 10 rpm and 0 kW burner power in a horizontal TBRC.

of the convective vortex remains equal to the initial slag temperature $T_{0,s}$. In Figure 13 this mid-vortex temperature is represented by T_{min} for 500 s < t < 1300 s and by T_{max} for t > 1500 s. At t = 1800 s slag solidification occurs primarily on interfaces with metal and refractory, resulting in formation of a freeze-lining. Thus, there is risk of slag solidification in this case. Regarding the vertical TBRC orientation, as it was already shown above, even with the maximum burner power of 600 kW, slag solidifies at the bottom of the pool due to stirring inefficiency. Even the presence of the additional heating at the metal-slag interface due to aluminothermic reduction is not enough to keep slag in a liquid state, see Figure 14. Note that 0 rpm case is modelled here as T_{min} and T_{max} are essentially independent of the rotation frequency in vertical TBRC, see Figure 9. All the above results are summarized in a 2D diagram of the occurrence of slag solidification depending on the burner power and on the TBRC inclination angle, see Figure 15 (left). On this diagram, the location of the border between the red zone ("Risk of slag solidification")

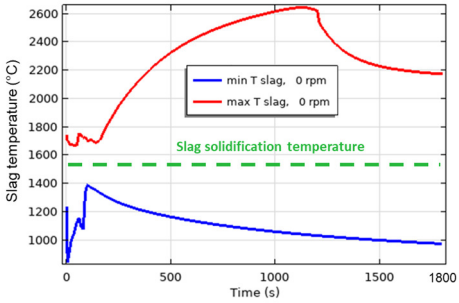

Figure 14. Maximum and minimum slag temperature at 0 rpm and 600 kW burner power in a vertical TBRC.

and the green zone ("Slag remains liquid") is defined by condition $T_{min} = T_{sol}$, where $T_{sol} = 1540°C$ is the slag solidification temperature, and T_{min} is the minimum slag temperature at $t = 1800$ s obtained by interpolation between available diagram points. Finally, if metal is not charged into TBRC, and only slag is present, then the absence of heat from the aluminothermic reduction is compensated by the increase of the burner power, which shifts the above diagram to the right, see Figure 15 (right).

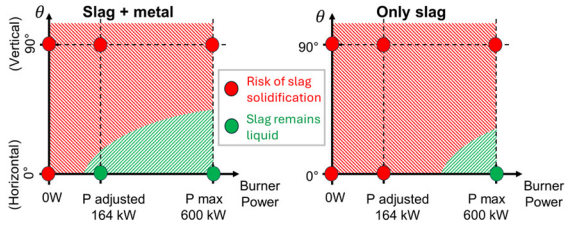

Figure 15. Occurrence of slag solidification depending on the burner power and on the TBRC inclination angle.

7. Conclusions

Numerical modelling of the top-blown rotary converter (TBRC) designed by MINTEK is presented. It is shown that the internal surface of TBRC can be preheated up to 1650°C in less than 30 min if useful burner power is 600 kW. Most of the thermal energy (81.2% in steady state) is lost by thermal radiation from inside of TBRC towards ambient environment through the opening at the top of TBRC. Thus, the use of a furnace lid is strongly recommended to prevent significant heat losses. The model of charged TBRC shows that horizontal TBRC orientation is the most favourable for charge stirring. As far as it rotates even at 1 rpm, the stirring is efficient for keeping slag in a liquid state. Contrary to that, in a vertically oriented TBRC stirring is not efficient at any rotation frequency (tested up to 20 rpm) and leads to slag solidification at the bottom of the pool. Even the maximum burner power of 600 kW together with the aluminothermic reduction heat is not sufficient to avoid slag solidification in a vertical TBRC. On the other hand, an optimum burner power of 164 kW exists in horizontal TBRC. This power together with the reaction heat is sufficient to keep slag in a liquid state during first 30 minutes of the process, if furnace is horizontally oriented. The occurrence of slag solidification depending on the burner power and on the TBRC orientation is summarized in 2D diagrams. This efficient decision-making tool makes part of the numerical support provided to the MINTEK's pilot campaign within the framework of the SisAl Pilot project.

References

[1] A. Jardy, *Modélisation mathématique et simulation numérique de procédé de refusion à l'arc sous vide,* 2005.

[2] A. Malhotra and S. S. Kang, "Turbulent Prandtl number in circular pipes," *International journal of heat and mass transfer,* vol. 27, no. 11, pp. 2158-2161, 1984.

[3] "NIST (Natioanl Institute of Standards and Technology) chemistry WebBook," [Online]. Available: https://webbook.nist.gov/chemistry/.

[4] M. Leitner, T. Leitner, A. Schmon, K. Aziz and G. Pottlacher, "Thermophysical Properties of Liquid Aluminum," *METALLURGICAL AND MATERIALS TRANSACTIONS,* vol. 48, no. 6, p. 3036–3045, 2017.

[5] M. J. Assael, I. J. Armyra, J. Brillo, S. V. Stankus, J. Wu and W. A. Wakeham, "Reference data for the density and viscosity of liquid cadmium, cobalt, gallium, indium, mercury, silicon, thallium, and zinc," *J. Phys. Chem. Ref. Data,* vol. 41, no. 3, p. 033101, 2012.

[6] J. Bohdansky and H. E. J. Schins, "Surface tension and density of the liquid earth alkaline metals Mg, Ca, Sr, Ba," *Journal of Inorganic and Nuclear Chemistry,* vol. 30, no. 9, pp. 2331-2337, 1968.

[7] J. Xin, L. Gan, L. Jiao and C. Lai, "Accurate density calculation for molten slags in SiO2-Al2O3-CaO-MgO systems," *ISIJ International,* vol. 57, no. 8, pp. 1340-1349, 2017.

[8] K. Tang, S. Gouttebroze, X. Ma, Q. Du and C. van der Eijk, "Representation of the multiphysical properties of SiO2-Al2O3-CaO slags by deep neural networks," in *Proceedings of the 16th International Ferro-Alloys Congress (INFACON XVI)*, (virtual), 2021.

[9] K. Tang, C. van der Eijk, S. Gouttebroze, Q. Du, J. Safarian and G. Tranell, "Rheological properties of Al2O3--CaO--SiO2 slags," *Calphad,* vol. 77, p. 102421, 2022.

[10] A. T. Dinsdale and P. N. Quested, "The viscosity of aluminium and its alloys--A review of data and models," *Journal of materials science,* vol. 39, pp. 7221-7228, 2004.

[11] K. C. Mills, L. Yuan and R. T. Jones, "Estimating the physical properties of slags.," *J. S. Afr. Inst. Min. Metall.,* vol. 111, no. 10, pp. 649-658, 2011.

[12] D. McEligot, W. D. Swank, D. L. Cottle and F. I. Valentin, "Thermal properties of G-348 graphite," *Idaho National Lab.(INL), Idaho Falls, ID (United States),* 2016.

[13] D. S. Smith, A. Alzina, J. Bourret, B. Nait-Ali, F. Pennec, N. Tessier-Doyen, K. Otsu, H. Matsubara, P. Elser and U. T. Gonzenbach, "Thermal conductivity of porous materials," *Journal of Materials Research,* vol. 28, no. 17, pp. 2260-2272, 2013.

[14] Entegris, Inc., *Properties and Characteristics of graphite, for the semiconductor industry.,* 2013.

[15] COMSOL Documentation, "Sutherland's law," [Online]. Available: https://doc.comsol.com/5.5/doc/com.comsol.help.cfd/cfd_ug_fluidflow_high_mach.08.27.html.

[16] G. K. Burgess and P. D. Foote, "The emissivity of metals and oxides. IV. Iron oxide," *Journal of the Washington Academy of Sciences,* vol. 5, no. 11, pp. 377-378, 1915.

Acknowledgements

Authors acknowledge the financial support under the Horizon 2020 European Union project SisAl Pilot, Grant Agreement N°869268.